Polymer Degradation and Stability 118 (2015) 45–58

Contents lists available at ScienceDirect

Polymer Degradation and Stability

journal homepage: www.elsevier.com/locate/polydegstab

Synthesis of a novel linear polyphosphazene-based epoxy resin and its application in halogen-free flame-resistant thermosetting systems

Huan Liu, Xiaodong Wang*, Dezhen Wu*

State Key Laboratory of Organic–Inorganic Composites, Beijing University of Chemical Technology, Beijing 100029, China

ARTICLE INFO

Article history:
Received 13 January 2015
Received in revised form
23 March 2015
Accepted 11 April 2015
Available online 21 April 2015

Keywords:
Linear polyphosphazene-based epoxy resin
Synthesis
Thermosetting systems
Flame retardant properties
Impact resistance

ABSTRACT

The synthesis of a novel linear polyphosphazene-based epoxy resin (*LPN*–EP) was performed via a six-step reaction pathway, and the chemical structures of the intermediate and target products were characterized by ^{1}H and ^{31}P NMR spectroscopy and Fourier transform infrared spectroscopy. A series of thermosetting systems consisting of diglycidyl ether of bisphenol–A and *LPN*–EP were prepared, and their mechanical properties, thermal stabilities, and flame retardant properties were investigated. The resulting thermosets exhibited excellent flame resistance with the UL–94 V-0 rating but also achieved a significant improvement in impact toughness as a result of the incorporation of rubbery *LPN*–EP. The thermosets also showed a good thermal stability highlighted for high char yields. The mechanism study indicates that the synergistic effect from the combination of phosphorus and nitrogen in polyphosphazene segments could effectively enhance the flame retardancy by acting in both condensed and gaseous phases to promote the formation of intumescent phosphorus-rich char on the surface of the thermosets. Such a char layer plays a role of insulating protective shell to prevent the volatiles from transferring to the surface of the thermosets as well as to shield the heat and oxygen diffusion, thus resulting in a self-extinguishing flame rating.

1. Introduction

There is a greatly concern about the emission of hazardous substances and the resulting environmental pollution with an increasing demand for new fire-resistant materials for the industrial and civil applications. As one of the most important functional materials with immanent flame retardancy, the brominated epoxy resin has been widely used for the electronic and electrical manufactures because of its outstanding characteristics such as high mechanical strength, good thermal and chemical stabilities, high flame resistance up to UL–94 V-0 rating, superior electrical insulating performance, and low shrinkage on cure [1–3]. Although such a traditional flame-retardant epoxy resin was well developed to meet the considerable secure requirements against the fire hazard, it unfortunately generated an environmental impact because of the production of super toxic brominated dibenzodioxins and dibenzofurans during combustion [4,5]. These halogenated substances with potential carcinogenicity not only are very harmful to human health but also bring pollution disasters when released into the environment [6,7]. In recent years, the use of halogen-containing materials in electrical appliances and electronic equipments has been legislatively restricted by the European Union according to the Restriction of Hazardous Substances (RoHS), and some of the brominated flame retardants were banned from the European Union market. Meanwhile, the World Health Organization and the US Environmental Protection Agency also recommended exposure limits and risk assessment of halogenous compounds to promise meeting the global sustainable development goals [8,9]. Therefore, the research and development of halogen-free fire-resistant epoxy resin have been attracting the increasing attention from both the scientific and industrial communities.

The design and synthesis of the epoxy resins containing phosphorus- or nitrogen-containing or both were considered as an effective pathway to gain flame retardancy for the resultant polymers as well as to avoid the use of halogenated components [10–12]. In past decades, many studies declared the realization of such a strategy through tailoring the epoxy-based macromolecules from backbones to side groups by incorporation of

* Corresponding authors. Tel.: +86 10 6441 0145; fax: +86 10 6442 1693.
E-mail addresses: wangxdfox@aliyun.com (X. Wang), wdz@mail.buct.edu.cn (D. Wu).

http://dx.doi.org/10.1016/j.polymdegradstab.2015.04.009
0141-3910/

phosphine oxide, phosphates, and the other phosphorylated and phosphonylated derivatives [13–18], because organophosphorus moieties are efficient radical scavengers and flame quenching agents. These studies also indicated that the combination of phosphorus-containing epoxy resins and nitrogen-based hardeners could lead to a dramatically high flame-resistant efficiency due to the phosphorus–nitrogen synergistic effect based on a condensed-phase mechanism involving polymer charring and a gaseous-phase flame-inhibition mechanism by removing the heat and diluting the combustible materials during fire process [19–24]. There is no doubt that the synthesis of reactive flame-retardant polymers can provide permanent flame retardancy for the epoxy curing system as well as maintains the original physical properties in a better way [13,19]. However, these phosphorus-containing epoxy systems hardly gain a high weight fraction of phosphorus, resulting in a low degree of flame retardancy [25,26]. There is still a challenge involving the achievement of high mechanical performance and effective flame retardancy at the same time. Therefore, the increasing focus on these issues has drawn the attention to the redesign of the epoxy macromolecules with more effective flame retardancy as well as better mechanical properties.

The epoxy resins containing cyclotriphosphazene group have recently attracted a great interest. It is well known that the phosphazenes present the alternating phosphorus and nitrogen atoms in a conjugative mode [27,28]. Such a unique chemical structure offers the synergism of the phosphorus–nitrogen combination resulting in outstanding flame retardancy and thus causes the originally highly flammable organic materials with auto-extinguishing [29,30]. This feature makes phosphazenes particularly good candidates as the flame-retardant materials for electric and electronic applications. A literature survey indicates that there are several investigations focused on the design and synthesis of the flame-retardant epoxy polymers with cyclotriphosphazene moieties in star-like, cyclolinear, spirocyclic, and cyclomatrix structures [31–35]. Nevertheless, the chemical incorporation of cyclotriphosphazene rings into the epoxy resins hardly achieved a high phosphorus/nitrogen content because of their steric effect, which may also lead to a high brittle nature of the resultant polymers [36]. The goal of this work is to design a novel epoxy curing system containing linear polyphosphazene moieties for halogen-free flame resistance. The linear polyphosphazene segment not only has the high phosphorus/nitrogen content resulting in excellent flame retardancy but also can generate a toughening effect for the resultant epoxy thermosets due to its rubbery nature. The synthesis and characterizations of the intermediate and final products were described, and the non-isothermal curing behaviors, mechanical performance, thermal stability and flammability characteristics of this epoxy systems was also investigated.

2. Experimental section

2.1. Chemicals

Phosphorus pentachloride (PCl_5), ammonium sulfate [$(NH_4)_2SO_4$], *4*-hydroxybenzaldehyde, sodium hydride (NaH, 70% suspension in mineral oil), phenol, sodium borohydride ($NaBH_4$), hexadecyl trimethyl ammonium bromide (CTAB), epichlorohydrin, *4,4′*-Diamino-diphenylmethane (DDM), tetrahydrofuran (THF), tetrachloroethane (TCE), methyl alcohol (MA), and *n*-hexane were all purchased from Beijing Chemical Reagent Co., Ltd., China. Diglycidyl ether of bisphenol–A (DGEBA) with an epoxy equivalent weight (EEW) of 187 g/equiv. was kindly provided by Wuxi Resin Factory of BlueStar New Chemical Materials Co., Ltd., China. The solvent, THF, was distilled from sodium benzophenone ketal prior to use, and the other chemicals and reagents were used as received.

2.2. Synthesis and reactions

The linear polyphosphazene-based epoxy resin (*LPN*–EP) was synthesized via six-stage reactions. In a typical process: a 1000-mL four-neck round-bottom flask equipped with a thermometer, a reflux condenser, a nitrogen inlet, and a mechanical stirrer was charged with 440 mL of TCE, 166.4 g of PCl_5, and 21.6 g of $(NH_4)_2SO_4$, and the mixture was heated to 145 °C with stirring for 1.5 h. After the reaction was completed, the reactant mixture was filtered, and the solvent was removed on a reduced pressure rotary evaporator, leaving a colorless oil of *N*-(dichlorophosphoryl)-*P*-trichloromonophosphazene (87.48 g, yield 99.4%) as product ***1***.

The product ***1*** was added into a three-neck round-bottom flask to perform polymerization at 245 °C for 2 h under a nitrogen atmosphere. A dark brown rubbery poly(dichlorophosphazene) as product ***2*** was obtained after removing by-products. The product ***2*** (40.0 g) was dissolved in 500 mL of THF to form a clear solution, and then sodium 4-formylphenolate (19.88 g) obtained from the reaction of 4-hydroxybenzaldehyde with NaH was added to this solution to perform a reaction at 65 °C for 6 h under a nitrogen atmosphere. Then, the reactant mixture was filtered, and the solvent was removed on a reduced pressure rotary evaporator, leaving a brown rubbery polymer of $[NP(OC_6H_4CHO)Cl)_{0.4}(NPCl_2)_{0.6}]_n$ as product ***3***. In succession, the product ***3*** (51.8 g) was dissolved in 500 mL of THF, and then sodium phenoxide was added into this solution to perform a reaction at 70 °C for 24 h. After the reaction was completed, the resultant mixture was filtered, washed repeatedly with the aqueous solution of $NaHCO_3$ and hot water, and then dried with anhydrous Na_2SO_4. After the solvent was removed by rotatory evaporation under reduced pressure, a off-white rubbery polymer of $[NP(OC_6H_4CHO)\ (OPh))_{0.4}(NP(OPh)_2)_{0.6}]_n$ as product ***4*** was obtained.

The product ***4*** (40.0 g) was dissolved in 500 mL of THF/methanol (1:1) mixture, and then 2.6 g of $NaBH_4$ was added. The reaction suspension was stirred at room temperature for 24 h. After the reaction was completed, the solvent was removed by rotatory evaporation, and then the resultant suspension was filtered, washed repeatedly with hot water, and then dried with anhydrous Na_2SO_4. After the solvent was removed by rotatory evaporation under reduced pressure, a off-white rubbery polymer of $[(NP(OC_6H_4CH_2OH)(OPh))_{0.4}(NP(OPh)_2)_{0.6}]_n$ was obtained as product ***5***. A 500-mL three-neck round-bottom flask equipped with a mechanical stirrer, a reflux condenser, and a nitrogen inlet was charged with 99.9 mL of epichlorohydrin, 75.0 g of product ***5***, and 1.9 g of CTAB as a catalyst. The mixture was heated to 70 °C with stirring for 3 h, and then an aqueous solution of NaOH (12.6 mL, 40 wt.%) was added. The reaction was continuously performed with stirring at 85 °C for 3 h. After the reaction was completed, the rotatory evaporation was performed under reduced pressure to remove the solvents and unreacted reagents. The resultant mixture was washed repeatedly with hot water, filtered, and then dried under vacuum. Finally, a light yellow solid was obtained as *LPN*–EP.

2.3. Preparation of thermosetting systems

A conventional epoxy resin (DGEBA) was homogeneously mixed with different loadings of *LPN*–EP in THF at room temperature, and then DDM as a hardener was added according to a stoichiometric amount of 1:1 for epoxy curing systems. *2,4,6*-Tris(dimethylaminomethyl) phenol (0.3 wt.%) as a curing accelerator was also added into the curing system. The resultant mixtures were kept in a

vacuum oven at 50 °C to remove the solvent. The thermal curing was performed at 150 °C for 3 h and then at 180 °C for 2 h. The resulting thermosets were cooled gradually to the ambient temperature to avoid stress cracking. Ultimately, the thermosets were achieved as some brown specimens with different shapes required for the mechanical and flame-retardant tests.

2.4. Characterization

^{1}H and ^{31}P Nuclear magnetic resonance (NMR) spectroscopy was performed on a Bruker AV-400 400 MHz spectrometer using deuterochloroform ($CDCl_3$) as a solvent. Solid-state ^{13}C NMR spectrum of the residual char after vertical burning experiment was obtained on a Bruker AV-300 300 MHz spectrometer. *Fourier*-transform infrared (FTIR) spectroscopy was performed on a Nicolet iS5 FTIR spectrophotometer at a scanning number of 32 using a KBr sampling sheet. The average molecular weight was obtained through steric exclusion chromatography (SEC) using a Water GPC515–2410 gel permeation chromatographer with THF as solvent at a flow rate of 1.0 mL/min. The weight per epoxy equivalent (WPE) of the synthesized *LPN*–EP was determined by the perchloric acid/tetra-athylammonium bromide method according to the Chinese national standard of GB/T 4612–2008.

The non-isothermal curing study was performed on a TA Instruments Q20 differential scanning calorimeter at different scanning rates under a nitrogen atmosphere. Thermogravimetric analysis (TGA) measurement was performed on a TA Instruments Q50 TGA analyzer at a heating rate of 10 °C/min under both nitrogen and air atmospheres. TG–FTIR spectroscopy combined measurement was performed on a Mettler Toledo TGA/DSC 1 STARe System coupled with a Nicolet 6700 FTIR spectrometer equipped with an *IR* gas cell. Limiting oxygen index (LOI) measurement was performed on an HD–2 oxygen index apparatus with a magneto-dynamic oxygen analyzer according to ASTM D–2863. The vertical burning tests were performed according to UL–94 standard, and the specimens were tailored in accordance with the dimensions as described in ASTM D–618 standard. The notched Izod impact test was performed on a SANS ZBC–1400A impact tester equipped with a pendulum of 1.25 J according to ASTM–D256 standard. The critical stress intensity factor as a fracture toughness parameter was measured and calculated by a three-point bending method using a SANS CMT–4104 universal test machine according to ASTM E–399 standard. Tensile and flexible tests were measured using the SANS CMT–4104 universal testing machine with a load cell of 10 kN capacity according to ASTM–D638 and D790 standards, respectively. Scanning electron microscopy (SEM) was performed on a Hitachi S–4700 scanning electron microscope coupled with an energy-dispersive X-ray (EDX) spectrometer. The fracture surfaces of the impact-fractured bars and the residual char after vertical burning tests were made electrically conductive by sputter coating with a thin layer of gold–palladium alloy before the SEM observation.

3. Results and discussion

3.1. Synthesis and characterizations

The synthesis of *LPN*–EP was performed through six step reactions, and the overall reaction sequences were illustrated in Schemes 1–6. The ^{31}P NMR spectroscopy was performed to monitor the reaction processing and also to confirm the expected chemical structures of the intermediate and final products. Fig. 1 shows the corresponding ^{31}P NMR spectra. The product ***1*** was obtained from the reaction of PCl_5 with $(NH_4)_2SO_4$ (see Scheme 1), and its ^{31}P NMR spectrum presented two doublet resonance signals

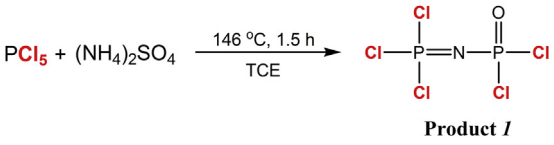

Scheme 1.

at δ = −11.22, and −3.28 ppm. The further polymerization of product ***1*** gave product ***2***, whose ^{31}P NMR spectrum showed an intensive singlet resonance signal at δ = −18.2 ppm corresponding to the phosphorus atom on the (−*P=N−) units of the linear polymer. The SEC characterization indicates that this linear polymer has a number-average molecular weight of 101,607. As shown in Scheme 3, the product ***3*** was synthesized through the partial substitutions of chloride atoms on product ***2*** with −(OC_6H_4CHO) groups. The different chemical environments at the phosphorus centers for product ***3*** resulted in four resonance signals in the ^{31}P NMR spectrum. The assignments for these resonance signals are explicated in the inserted graph of Fig. 1. The product ***4*** was obtained by the substitutions of remainder chloride atoms on product ***3*** with phenolic groups (see Scheme 4). Two resonance signals were observed in the ^{31}P NMR spectrum of product ***4*** and were well assigned to the phosphorus atoms on the linear polymer with different substituent environments as marked in the inserted graph of Fig. 1. The product ***4*** was reacted with $NaBH_4$ to give product ***5*** (see Scheme 5), and then the target product was achieved by the reaction of product ***5*** with epichlorohydrin in the presence of CTAB as a catalyst (see Scheme 6). Own to the minor change in the substituent environment of phosphorus atoms, the resonance signals for the target product and product ***5*** are almost identical in their ^{31}P NMR spectra. Products ***4*** and ***5***, and target product were also confirmed by ^{1}H NMR spectroscopy. Although the resonance signals for these three products are complicated in the ^{1}H NMR spectra as shown in Fig. 2, they are assigned well to all the protons on the molecular chains of these products as labeled and depicted the inserted graphs of Fig. 2.

Furthermore, the chemical structure of the target product was confirmed by FTIR spectrum shown in Fig. 3. The spectrum of the target product shows a characteristic absorption at 1243 cm^{-1} due to the P=N group. The two characteristic peaks at 1180 and 830 cm^{-1} are attributed to the vibrations of P–O–Ar and P–N bonds, respectively. Two intensive absorption peaks at 937 and 763 cm^{-1} corresponding to C–O–C stretching vibration provide the evidence for the introduction of epoxy groups. The absorption band at 3452 cm^{-1} is attributed to the hydrogen-bonded O–H stretching, indicating that ring-opening reaction of partial epoxy groups. As an important feature of the spectrum, the characteristic peaks about $-CH_2-$ and −CH− stretching vibrations were observed at 2964, 2922, and 2865 cm^{-1}. In addition, the characteristic absorptions at 3047, 1607, 1508 cm^{-1} are representative of the aromatic C–H, C–C, and C=C stretching vibrations. The characteristic absorption peaks in the spectrum indicated that the chemical compositions of the target product were expected as *LPN*–EP. The analysis of the target product by SEC shows that *LPN*–EP has a number-average

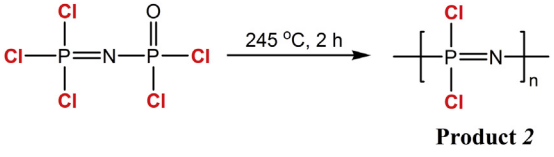

Scheme 2.

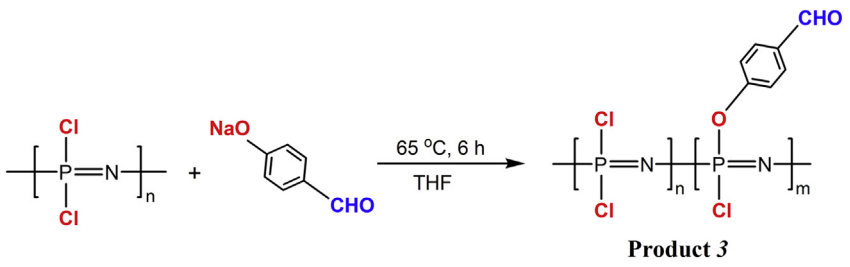

Scheme 3.

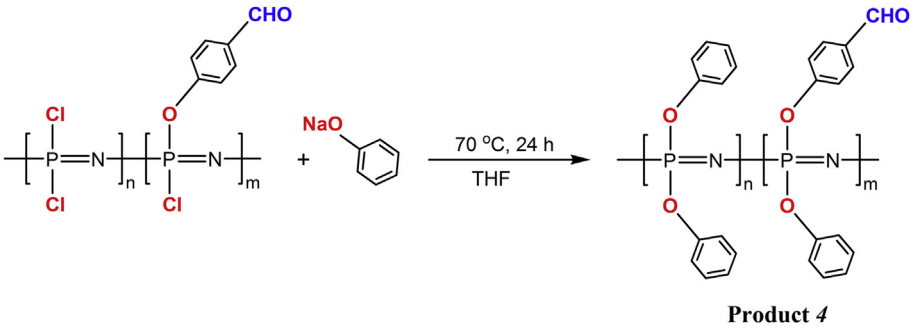

Scheme 4.

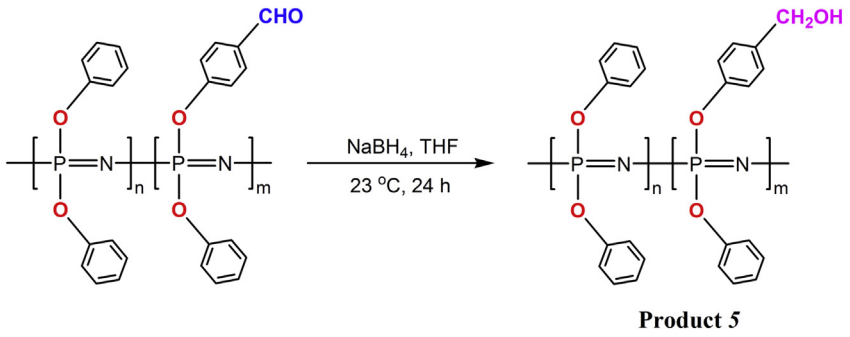

Scheme 5.

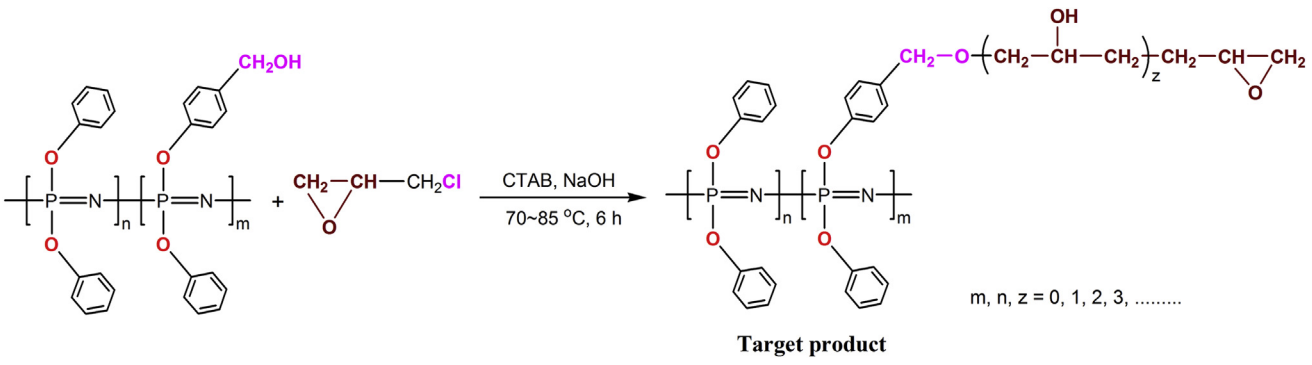

Scheme 6.

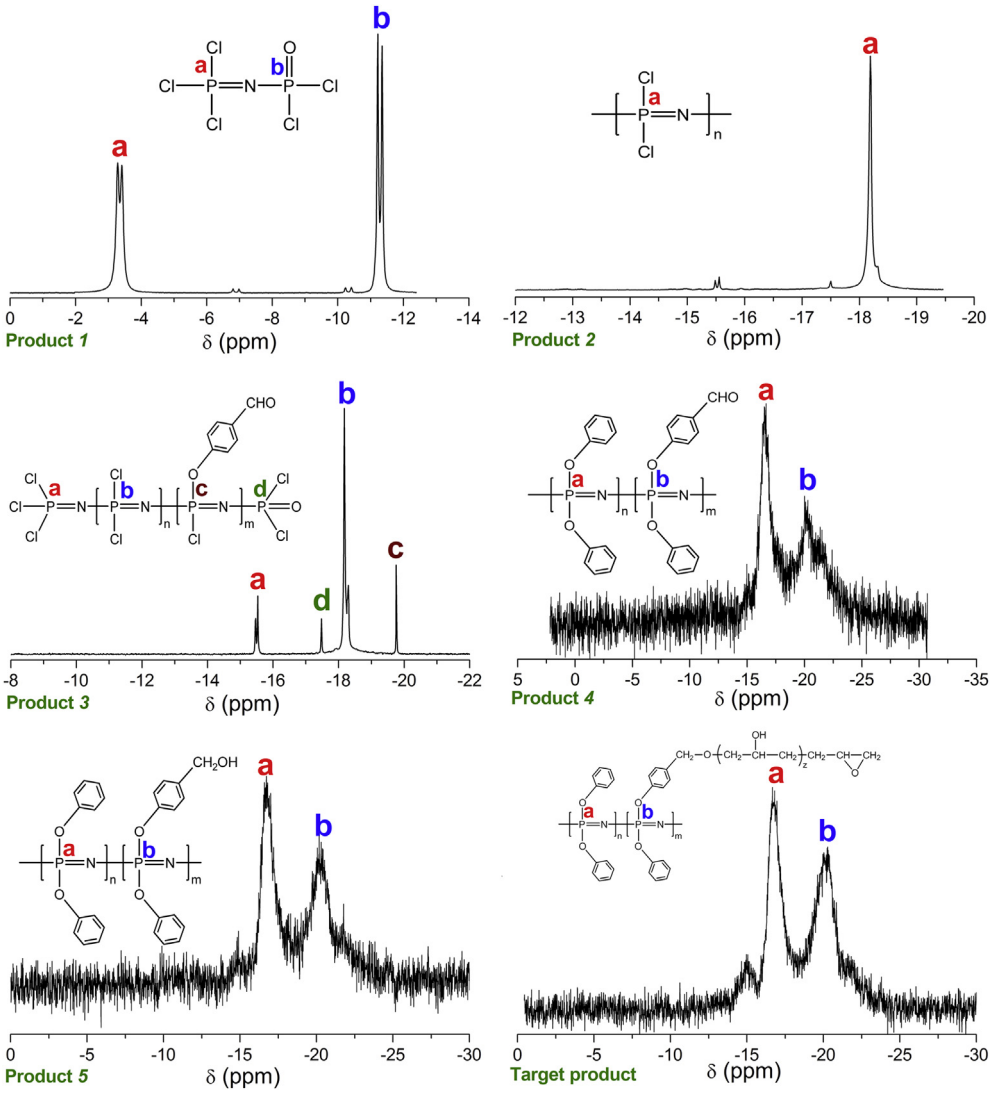

Fig. 1. ^{31}P NMR spectra of intermediate products and *LPN*–EP.

molecular weight no more than 186,325 and a weight-average molecular weight of 374,514. The WPE of *LPN*–EP were also determined by the perchloric acid–tetraathylammonium bromide method and presented a value of 671.4 g/equiv.

3.2. Curing kinetics

The resultant *LPN*–EP was mixed with a conventional epoxy resin, DGEBA, and DDM as a harder to constitute a series of thermosetting systems, and the dynamic DSC scans were performed to investigate their curing behaviors. Fig. 4 shows the non-isothermal DSC curves for these curing systems at different scanning rates. Both DGEBA and DGEBA/*LPN*–EP thermosetting systems exhibit a single exothermic peak at a low scanning rate of 5 °C/min, indicating that the curing reactions originated from a single chemical process of the epoxy groups on DGEBA and *LPN*–EP with the hardener. It is interestingly observed that the thermosetting systems containing 10 and 20 wt % of *LPN*–EP show a bimodal curing behavior at higher scanning rates. This is attributed to the non-isochronous curing between *LPN*–EP and DGEBA caused by different reactivity of epoxy groups on the two polymers. However, the thermosetting systems containing 30 wt % of *LPN*–EP presents a single curing peak on its DSC curve. This may be due to the heat release of thermal curing of *LPN*–EP in advance of the curing reaction of DGEBA, which accelerates the curing of DGEBA with the hardener and results in a shift of exothermic peak temperature (T_p) toward a low temperature. The dynamic DSC results could optimize the curing technology for the manufacturing process of these curing systems, and the optimal curing temperatures could be determined by a linear fitting method in terms of the T_p [31].

The curing kinetics of DGEBA/*LPN*–EP curing systems were also investigated in order to develop and optimize the curing technology for the manufacturing process of this new epoxy material. Assuming the heat flow is proportional to the change in the extent of curing reaction for an epoxy thermosetting system, the curing extent (α) can be expressed by a single step kinetic equation:

$$\frac{d\alpha}{dt} = \frac{1}{\Delta H_0}\frac{dH}{dt} \quad (1)$$

where $d\alpha/dt$ is the curing reaction rate, dH/dt the rate of heat, and ΔH_0 the curing heat of overall curing reaction, which can be

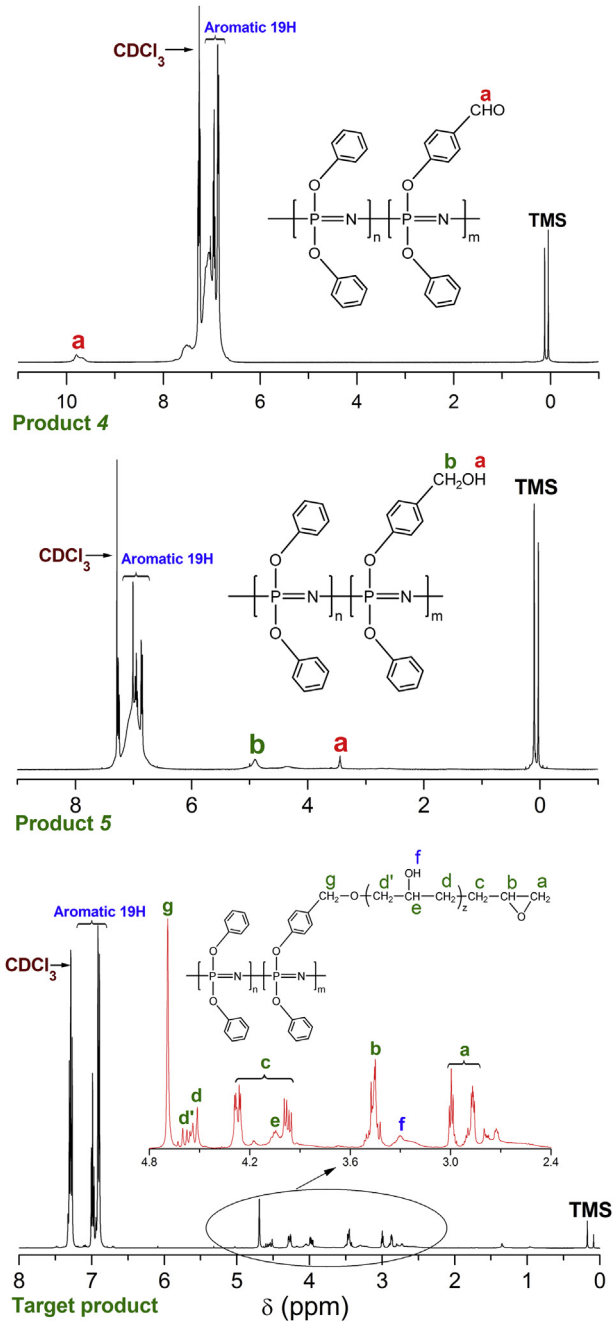

Fig. 2. ^{1}H NMR spectra of intermediate products and *LPN*–EP.

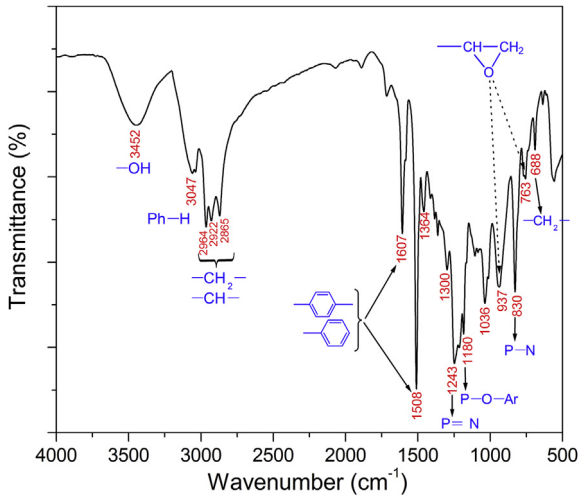

Fig. 3. FTIR spectrum of *LPN*–EP.

calculated through the integral of the curing DSC curve. In this case, most curing processes is commonly described by the following equation [37,38]:

$$\frac{d\alpha}{dt} = A\exp\left(-\frac{Ek}{RT}\right)f(\alpha) \tag{2}$$

where A is the frequency factor, E_k the activation energy of curing reaction, R the gas constant, T is the absolute temperature, and $f(\alpha)$ the function representing the kinetic model. For the DGEBA/*LPN*–EP systems under the non-isothermal curing condition, their activation energy could be deduced from the slope of the plot of $\ln(\beta/T_p^2)$ versus $1/T_p$ on the basis of the well-known Kissinger–Akahira–Sunose (KAS) method [39]:

$$-\ln\left(\frac{\beta}{T_p^2}\right) = \frac{E_k}{RT_p} - \ln\frac{AR}{E_k} \tag{3}$$

where β is the heating rate. Fig. 5 shows the curves of $\ln(\beta/T_p^2)$ versus $1/T_p$ for the DGEBA/*LPN*–EP curing systems at different weight ratios, and calculated kinetic parameters are listed in Table 1. It is noted that the activation energy of the DGEBA/*LPN*–EP curing systems are significantly higher than that of the DGEBA one. Although the *LPN*–EP has a flexible molecular chain, there are numerous aromatic groups on its chain, which can generate the steric hindrance. In this case, the potential barrier of the curing reaction for the DGEBA systems was increased in the presence of *LPN*–EP, thus resulting in the higher activation energy. Málek method was usually used to find an appropriate kinetic model, which can describe the conversion function of the curing reaction in a best way [37,40,41]. According to málek method, it is necessary to appeal to the functions of $y(\alpha)$ and $z(\alpha)$:

$$y(\alpha) = \exp(u)\left(\frac{d\alpha}{dt}\right) \tag{4}$$

$$z(\alpha) = \pi(u)\left(\frac{d\alpha}{dt}\right)\frac{T}{\beta} \tag{5}$$

where u is E_k/RT, $\pi(u)$ the expression of temperature integral, and u can be approximately calculated by the fourth-order rational expression proposed by Yang et al. [42]. with the following equation :

$$\pi(u) = \frac{(u^3 + 18u^2 + 88u + 96)}{(u^4 + 20u^3 + 120u^2 + 240u + 120)} \tag{6}$$

Fig. 6 shows $y(\alpha)$ and $z(\alpha)$ versus α for the DGEBA/*LPN*–EP curing systems at a heating rate of 5 °C/min. According to the curves shown in Fig. 6, α_M and $\alpha^{\infty}{}_p$ are the values of α corresponding to the maximum of $y(\alpha)$ and $z(\alpha)$, respectively, and these values are collected in Table 1. It is noteworthy that the value of α shows a variation trend of $\alpha_p^{\infty} > \alpha_M > 0$, and meanwhile, the values of α_p^{∞} for these curing systems is lower than 0.632. This value was considered as a characteristic 'fingerprint' and could test the

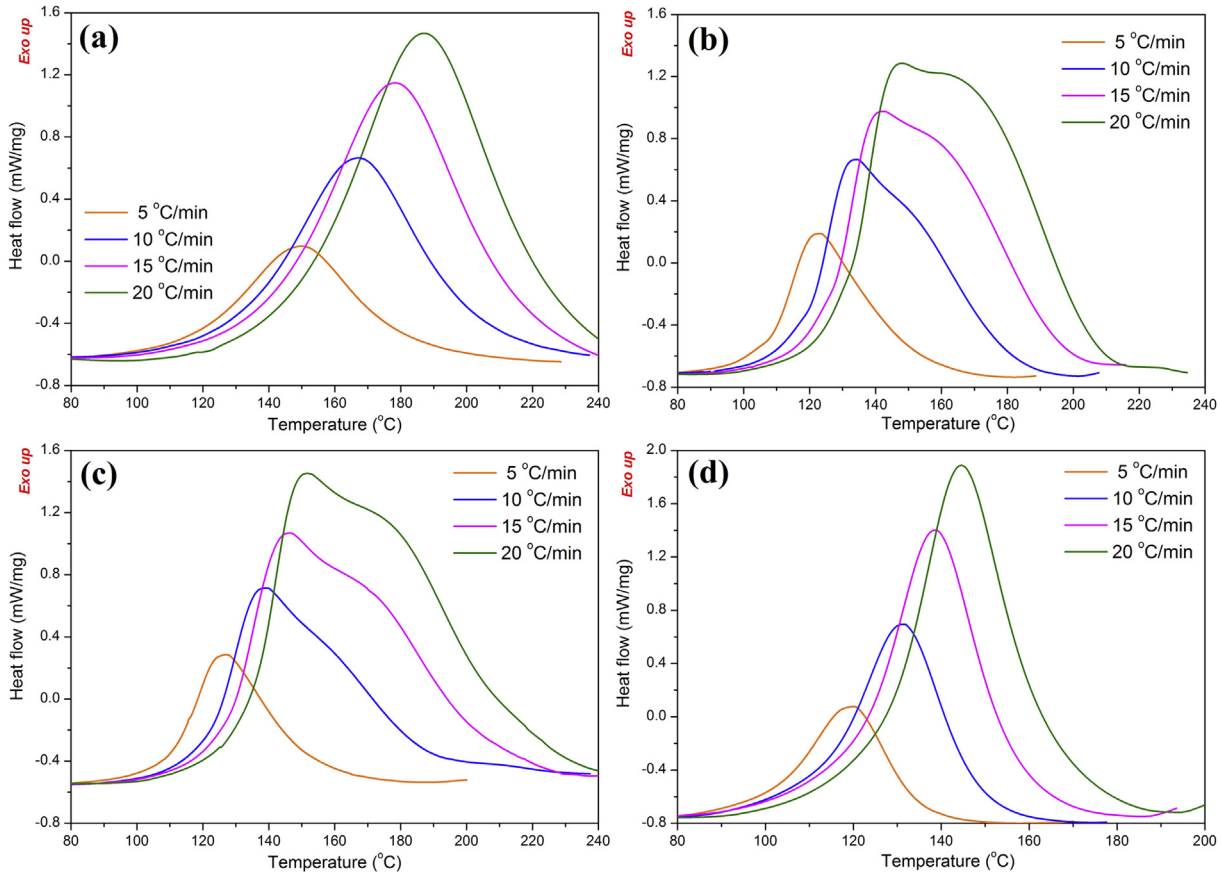

Fig. 4. DSC curves of the thermal curing for DGEBA/*LPN*–EP thermosetting systems at weight ratios of (a) 100/0, (b) 90/10, (c) 80/20, and (d) 70/30.

applicability of this model according to Málek's experience [35]. The above results implied the curing reactions of the DGEBA/*LPN*-EP systems could be described by the Šesták–Berggren (*m*,*n*) model as follows [43]:

$$\frac{d\alpha}{dt} = A\exp\left(-\frac{Ek}{RT}\right)\alpha^m(1-\alpha)^n \quad (7)$$

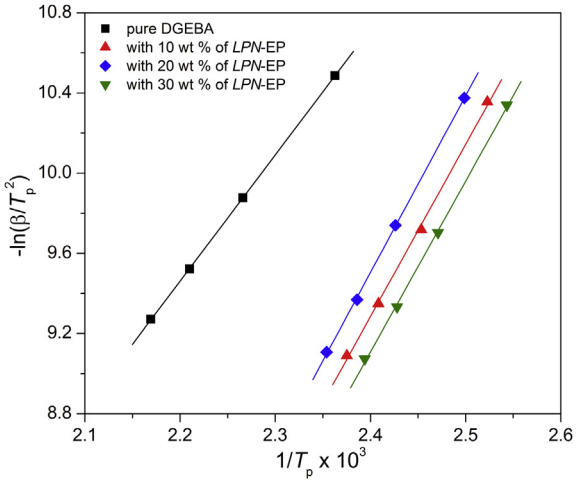

Fig. 5. The Kissinger's plots of $-\ln(\beta/T_p^2)$ versus $1/T_p$ for DGEBA/*LPN*–EP thermosetting systems.

where *m* and *n* are the kinetic exponents contributed by autocatalytic and non-autocatalytic reactions, respectively. According to a nonlinear least-squares fitting method, the kinetic parameters derived from the Šesták–Berggren model are summarized in Table 1. It should be pointed out that *A*, *m*, and *n* are almost independent of the heating rate, which is an indication that the curing mechanisms are independent of the heating rate [44]. The calculated results show the value of *m* is close to *n*, which means the contribution of non-autocatalytic reaction similar with autocatalytic reaction. Fig. 7 shows the plots of the experimental curing reaction rates and calculated fitting ones at different heating rates. It is demonstrated that most of the pure DGEBA and DGEBA/*LPN*–EP curing systems obtained a good agreement between the experimental and calculated data, and nevertheless, the deviation is also found in the DGEBA/*LPN*–EP curing systems at weight ratios of 90/10 and 80/20. This indicates that the employed Šesták–Berggren model could well describe the non-isothermal DGEBA/*LPN*–EP curing systems but is not so perfect to simulate the bimodal exothermic curing process. The maximum reaction rates under different scanning rates were all found to shift to lower temperatures with increasing the *LPN*–EP loading in the curing systems. This phenomenon indicates that the epoxide rings on the multifunctional *LPN*–EP as side groups have much higher chemical reactivity compared to those on the bifunctional DGEBA as end groups. Therefore, the increase of *LPN*–EP loading can enhance the curing reaction and reduce the curing temperature [45]. These investigated results will provide the necessary processing parameters for the thermal curing of the DGEBA/*LPN*–EP thermosetting systems.

Table 1
The curing kinetic parameters obtained from DSC analysis for the DGEBA/*LPN*–EP thermosetting systems.

Thermosetting system	β (°C/min)	T_p (°C)	E_k (kJ/mol)	a_M	Mean a_M	α_p^∞	Mean α_p^∞	ln$A$ (1/min)	m	n	R
Pure DGEBA	5	150.09	52.30	0.5065	0.5039	0.5429	0.5342	0.5186	1.138	1.115	0.9993
	10	168.18		0.5072		0.5537		0.8224	1.005	0.9847	0.9994
	15	179.33		0.5010		0.5268		1.129	1.010	0.9808	0.9992
	20	187.86		0.5008		0.5135		1.414	0.9782	0.9830	0.9992
DGEBA + 10 wt % LPN–EP	5	123.22	71.36	0.4055	0.3105	0.4338	0.4139	0.7492	0.9986	1.134	0.9923
	10	134.44		0.3185		0.3531		0.7721	0.7399	0.8622	0.9844
	15	142.06		0.2597		0.3208		0.9114	0.6808	0.7922	0.9871
	20	147.88		0.2584		0.5479		1.051	0.6596	0.7549	0.9880
DGEBA + 20 wt % LPN–EP	5	127.09	73.27	0.4557	0.3262	0.4817	0.3531	0.7539	0.9873	1.096	0.9944
	10	138.99		0.2984		0.3418		0.8467	0.7832	1.1323	0.9901
	15	145.96		0.2921		0.3038		0.8252	0.6699	0.8970	0.9854
	20	151.68		0.2565		0.2849		1.017	0.6576	0.8814	0.9861
DGEBA + 30 wt % LPN–EP	5	120.03	70.85	0.6003	0.5381	0.6174	0.5703	0.9457	1.267	0.9442	0.9987
	10	131.53		0.5452		0.5891		1.801	1.241	0.9777	0.9987
	15	138.70		0.5226		0.5583		2.771	1.230	1.063	0.9986
	20	144.56		0.4843		0.5163		3.534	1.176	1.129	0.9978

3.3. Mechanical performance

It is well known that the most commercial epoxy thermosets have a brittle nature despite of its high rigid feature due to a high crosslinking density. Therefore, in order to overcome this drawback and extend its application areas, the toughness of the epoxy resins is expected to be properly enhanced through some feasible pathways. The mechanical properties of the DGEBA/*LPN*–EP thermosets were evaluated and the obtained results were presented in Figs. 8 and 9. It is observed from Fig. 8 that the impact toughness of the thermosets exhibits a remarkable enhancement due to the incorporation of *LPN*–EP, and the notched impact strength of the thermoset containing 30 wt % of *LPN*–EP achieves an increment of 250% over the pure DGEBA thermoset. The three-point bending experiment reveals that the critical stress intensity factor (K_{1C}) is also significantly improved, and the values of K_{1C} indicated that the higher loading of *LPN*–EP leads to much better toughness for the thermosets. The *LPN*–EP was found to present rubbery state, and therefore, such a rubbery domain in the epoxy thermosets could toughen the brittle matrix by initiating the crazing or deformation or both. However, the presence of the rubbery *LPN*–EP inevitably reduced tensile and flexural strength of the thermosets as well as Yang's and flexural moduli as demonstrated by Fig. 9. It is understandable that the incorporation of *LPN*–EP into thermosetting systems not only can result in a decrease in elastic modulus of the thermosets but also generate some new interfaces between the rubbery domain and DGEBA matrix. This may lead to a reduction of the fracture stress when the tensile and bending loads are applied. Fig. 10 shows the morphologies of fracture surfaces of the impact specimens. The pure DGEBA thermosets was founded to presents a considerable smooth fracture surface, indicating a typical brittle fracture behavior under the notched impact. However, the impact-fractured surfaces the DGEBA/*LPN*–EP thermosets exhibit a rippling feature due to the matrix deformation, and such deformation become more and more significant with increasing the *LPN*–EP loading. Nevertheless, it is noteworthy that the *LPN*–EP domains as some small particles were homogeneously distributed in the epoxy matrix. These rubbery *LPN*–EP domains could initiate the remarkable matrix deformation when the matrix shear yielding occurred due to applied impact force, resulting in the dissipation of impact energy and further enhancing the impact toughness.

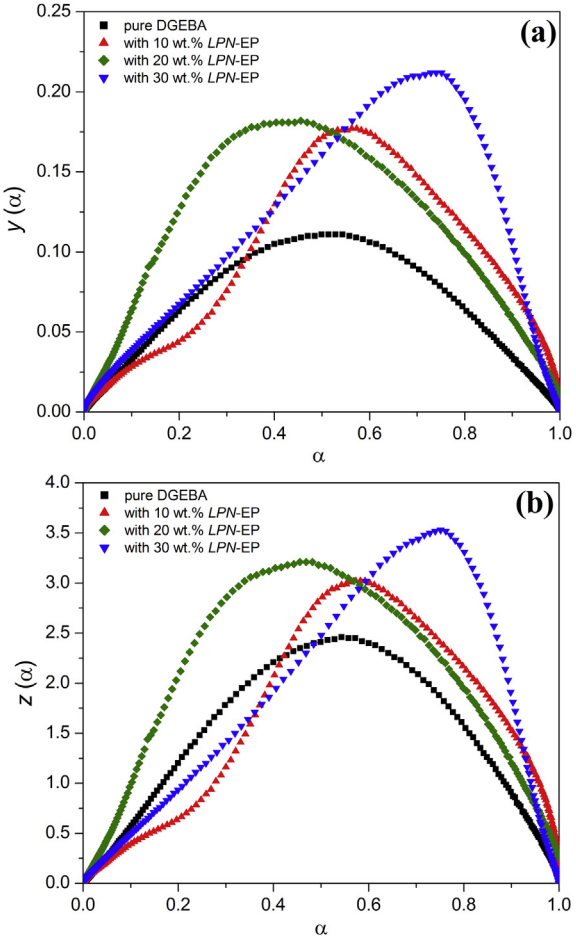

Fig. 6. Plots of the functions of $y(\alpha)$ and $z(\alpha)$ versus α for DGEBA/*LPN*–EP thermosetting systems at a heating rate of 5 °C/min.

3.4. Thermal stability

The thermal stability is considered as one of the most essential properties for an epoxy thermosetting system because it establishes a service environment for the designed thermosetting composites. The thermal stabilities of the DGEBA/*LPN*–EP thermosets were investigated by TGA under both nitrogen and air atmospheres. The obtained TGA thermograms are illustrated in Fig. 11, and the characteristic data of thermal degradation are collected in Table 2. Both the pure DGEBA and DGEBA/*LPN*–EP thermosets were found to exhibit a typical one-step degradation behavior in nitrogen but a two-stage decomposition in air. This is an

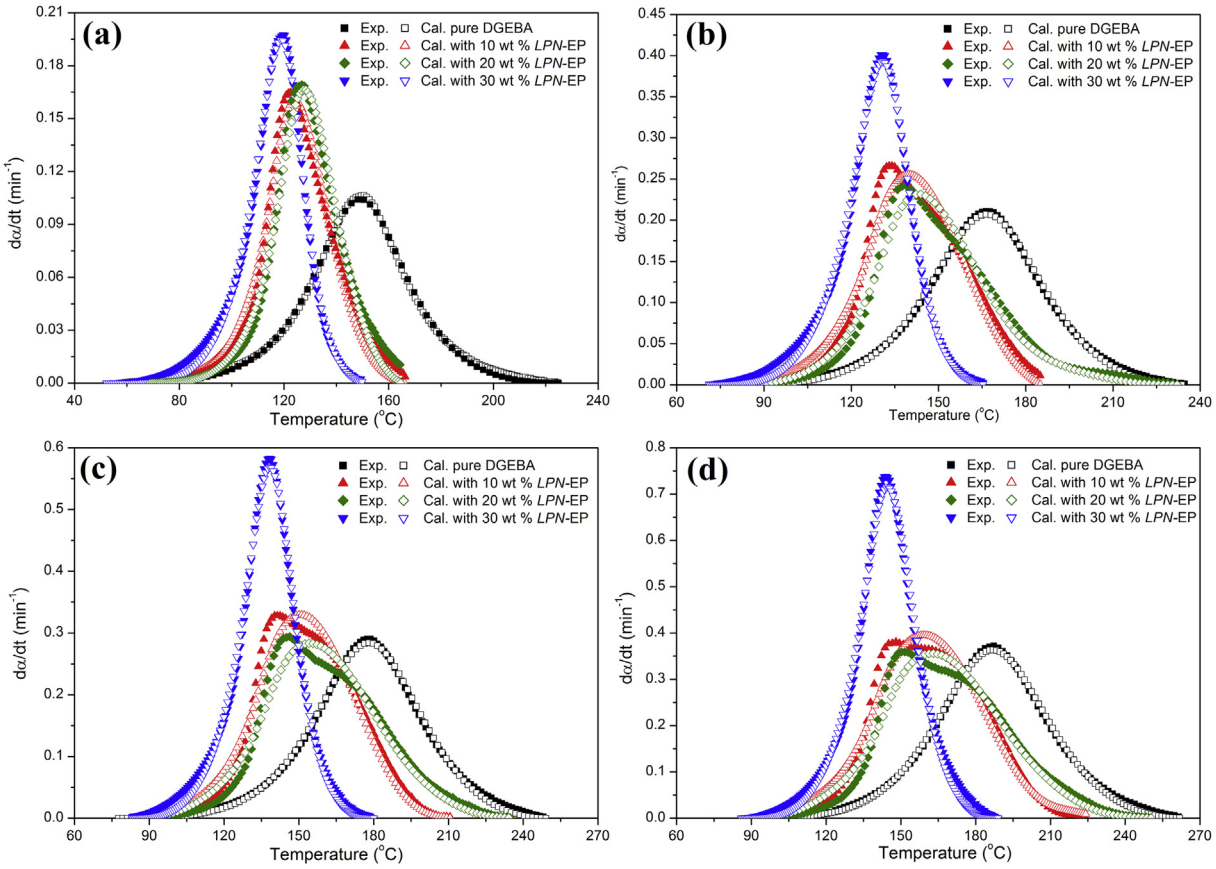

Fig. 7. Plots of the experimental curing reaction rates and calculated fitting ones for DGEBA/*LPN*–EP thermosetting systems at heating rates of 5, 10, 15, and 20 °C/min.

indication that these thermosetting systems underwent the pyrolysis in different ways under different atmospheres. The onset decomposition temperature (T_{onset}) defined as the temperature corresponding to 5% mass loss is usually considered as an indicator of thermal stability for a polymer. It is observed from Table 2 that all of the thermosets shows lower T_{onset}'s in air than in nitrogen as a result of the thermo-oxidation induced by the oxygen in air. Furthermore, the pure DGEBA thermoset shows a higher T_{onset} than the DGEBA/*LPN*–EP ones in all the cases. This is attributed to the decomposition of the less stable P–O–C bond in the side groups of *LPN*–EP [46,47]. Meanwhile, the characteristic temperature corresponding to the weight loss occurred at a maximum rate (T_{max}) also presents a similar variation trend with T_{onset} for all the thermosets. The lower T_{max} is due to the major degradation from the main chains of *LPN*–EP occurring prior to that of the DGEBA network. On the other hand, it is surprisingly noted that the DGEBA/*LPN*–EP thermosets achieved much higher char yields both in nitrogen and in air compared to the pure DGEBA one which almost obtained little residual char at the end of TGA test. Moreover, the char yield was found to increase with increasing the *LPN*–EP loading in the curing systems. It is understandable that a dense phosphorus-rich char is easily formed during the thermal and thermo-oxidative decompositions when the polyphosphazene segments are incorporated into the thermosetting system in a covalent way [48,49]. Such a feature can significantly promote the char formation of thermosets and thus increases the char yields of the resulting thermosets.

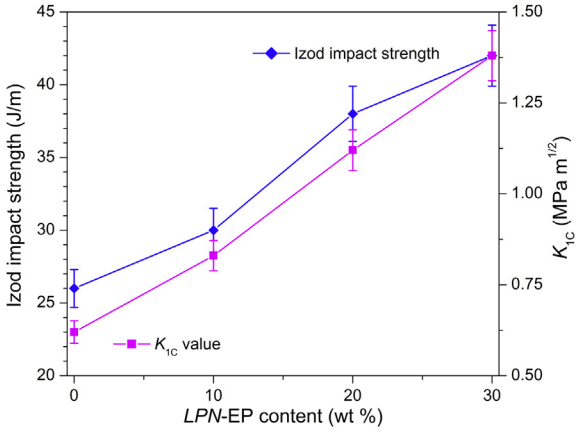

Fig. 8. Notched Izod impact strength and K_{1C} values of DGEBA/*LPN*–EP thermosets.

To understand the degradation mechanisms of the DGEBA/*LPN*–EP thermosets, the TG–FTIR spectroscopy was performed to investigate the evolution of gaseous products during their thermal decomposition. Fig. 12 shows the FTIR spectra of the evolved gases recorded at different temperatures during the TGA test in air. It is highlighted that two intense characteristic bands were observed at 677 and 2250–2380 cm^{-1}, indicating the formation of CO_2 in the entire pyrolysis process. This is attributed to the scission and the following thermo-oxidative decomposition of main segments of the thermoset. The presence of the N–H and O–H stretching vibrations at 3500–3800 cm^{-1} indicates the release of the amine-containing gases and oxidative fragments like water vapor as a result of the pyrolysis of phosphazene and hydrocarbon segments, respectively. The multiple absorption peaks at 1510–1550 cm^{-1}

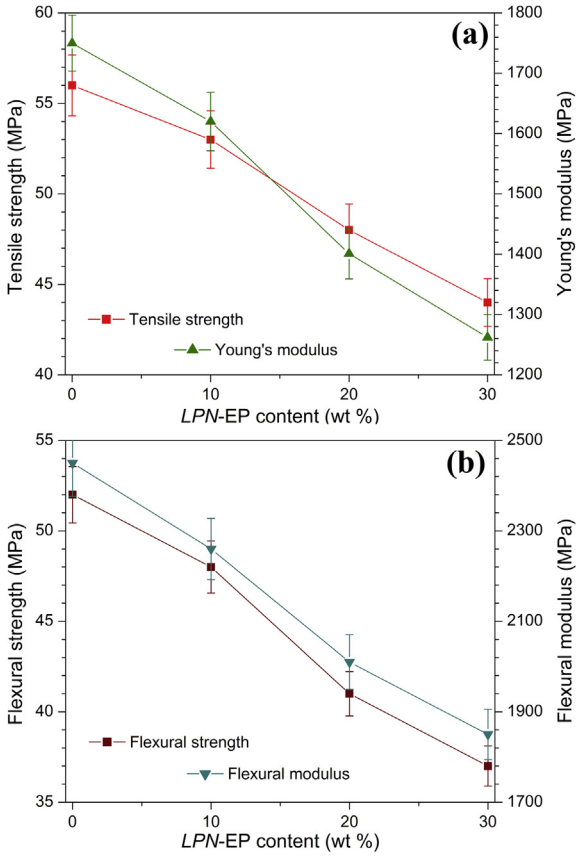

Fig. 9. Tensile and flexural properties of DGEBA/*LPN*–EP thermosets.

also confirm the release of the amine-containing gases. Moreover, the absorption peaks correspond to CO gas could be found at 2110 and 2180 cm^{-1} in the temperature range of 500–650 °C, which was ascribed to the lack of oxygen in the specimen cell during the rapid thermal decomposition of the thermosets at high temperatures.

3.5. Flame retardant property

The flame retardant properties of the DGEBA/*LPN*–EP thermosets were assessed by LOI and UL–94 vertical burning tests, and the obtained results were summarized in Table 2. As an indicator corresponding to the minimum oxygen concentration maintaining combustion of a material, the LOI can well describe the flammability characteristics of the thermosets. The pure DGEBA thermoset was found to have a low LOI of 22.3 vol %, and it also failed in the UL–94 vertical burning test, indicating a highly combustible nature. However, the DGEBA/*LPN*–EP thermosets were found to present the increasing values of LOI with increasing the *LPN*–EP loading, and the thermoset containing 30 wt % of *LPN*–EP obtained a high LOI up to 31.8 vol %. The UL–94 vertical burning tests also indicated that the thermosets achieved the V-1 rating at *LPN*–EP loadings of 10 and 20 wt % and further gained a self-extinguishing V-0 rating with increasing the *LPN*–EP loading to 30 wt %. Moreover, the flaming drippings were no longer observed due to the presence of *LPN*–EP. It is important to note that the flame-retardant performance of the thermosets is essentially dependent on the phosphorus content within the thermosets as indicated by the data in Table 2. Many studies show that the flame-resistant performance not only depends on the phosphorus content but also has a structural dependency of flame-retardant polymers [50–52]. Schäfer et al. reported that the epoxy thermosets containing 5,10-dihydrophenophosphazine-10-oxide needed 2.69 and 3.20 wt % of phosphorus element to reach the V-1 and V-0 ratings, respectively [53]. However, they found that the thermosets containing 9,10-dihydro-9-oxa-10-phosphaphenanthrene-10-oxide obtained the V-1 and V-0 rating at a phosphorus content of 2.15 and 2.63 wt %, respectively [53]. In this study, to reach the V-1 rating, the thermoset only needed a phosphorus content of 1.15 wt %, whereas, the thermoset containing 3.46 wt % phosphorus element could achieve the V-0 rating. In deed, we found that the thermoset containing 2.31 wt % of phosphorus element was standing on the border of the V-0 and V-1 ratings through the observation from the UL–94 vertical burning test. These results suggested that the incorporating small amount of *LPN*–EP could impart the elementary flame retardancy to the DGEBA thermosetting systems. Such a flame-resistant

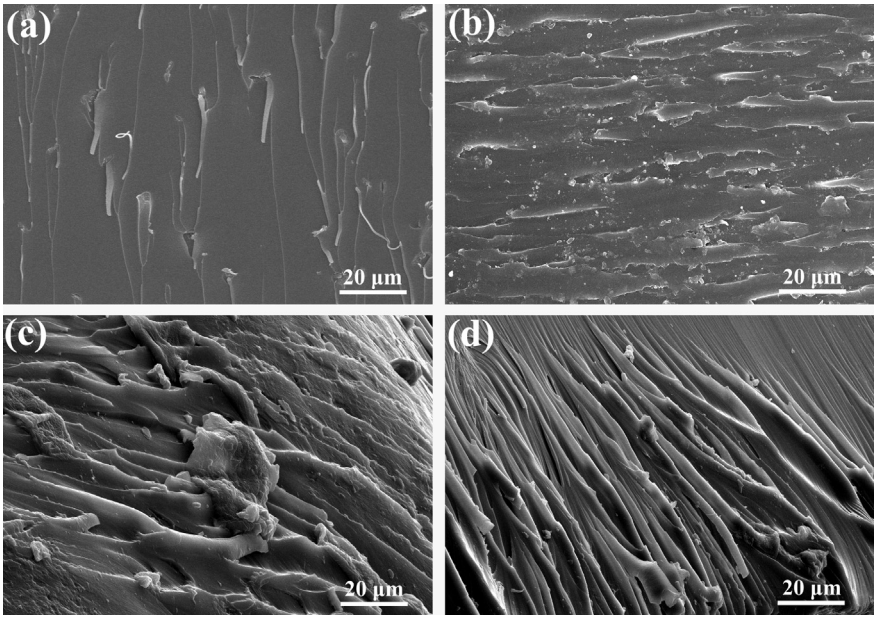

Fig. 10. SEM micrographs of impact-fractured surfaces of (a) the pure DGEBA thermoset and DGEBA/*LPN*–EP ones containing (b) 10 wt %, (c) 20 wt %, and (d) 30 wt % of *LPN*–EP.

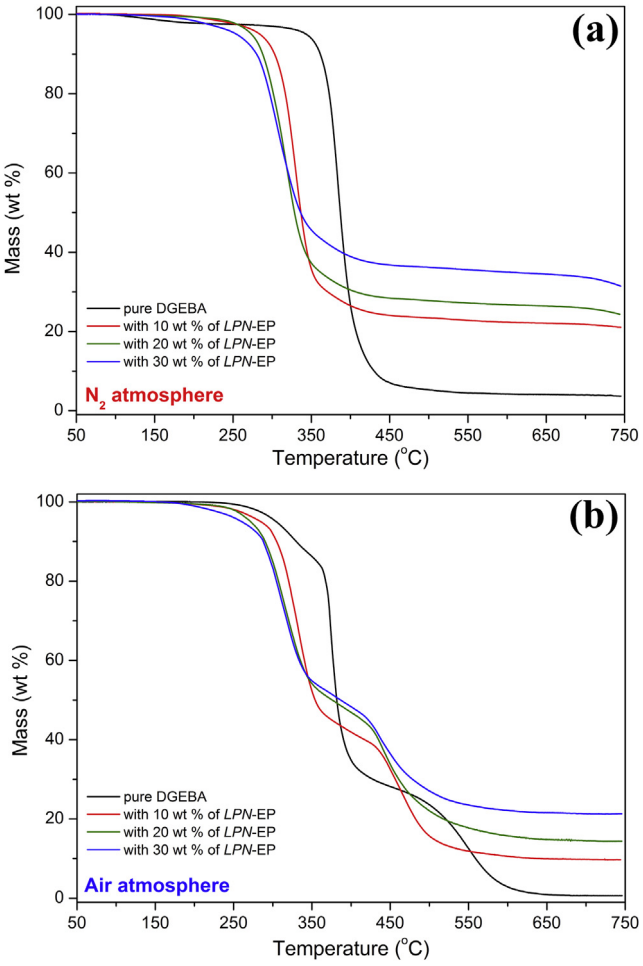

Fig. 11. TGA thermograms of DGEBA/*LPN*–EP thermosets.

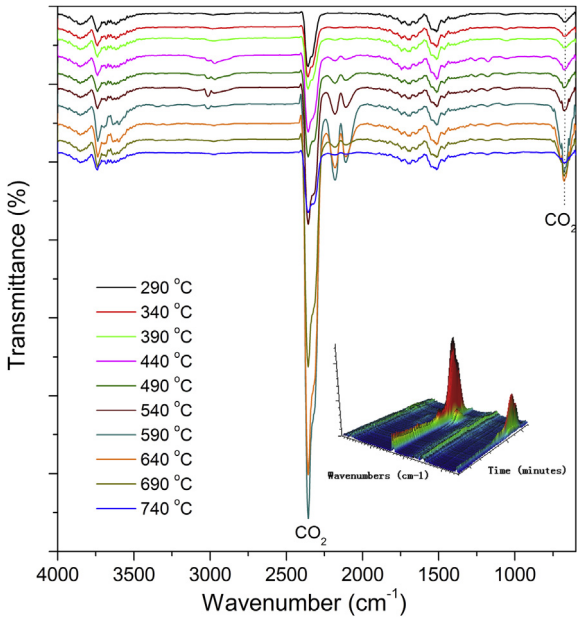

Fig. 12. FTIR spectra of the DGEBA/*LPN*–EP thermoset containing 30 wt % of *LPN*–EP recorded at different temperatures from TG–FTIR measurement.

feature assuredly results from the synergistic effect of phosphorus–nitrogen combination from polyphosphazene segments in the cured network [31–33]. Nevertheless, the phosphorus content is still necessary to be greatly increased within the thermosets for a high level of flame resistance.

According to the mechanisms of enhanced flame retardant performance by means of the phosphazene-based moieties [54,55], the presence of these polyphosphazene segments can promote the formation of residual char as an insulating protective layer preventing the volatiles from transferring to the surface of the materials and increases the thermal stability of char at higher temperatures. Meanwhile, the polyphosphazene can also release non-flammable nitrogen-containing gases or decompose endothermically to cool the pyrolysis zone at the combustion surface. In order to understand these mechanisms, the morphologies and chemical structures of residual char were intensively investigated. Fig. 13 shows the SEM micrographs of the residual char obtained from the test bar after vertical burning tests. The aspects of the residual char are observed to present not only a dense and compact surface but also a porous structure with seldom pores breaking-through, indicating the formation of intumescent char. It is noteworthy that the charring layer becomes more perfect with increasing the *LPN*–EP loading in the thermosets. Such a structural feature could impart a temperature grad to char layer during combustion and thus made the char layer well serve as a barrier against heat and oxygen diffusion to the surface of burning item [56]. Fig. 14 shows the FTIR spectra of the residual char left from the vertical burning tests. The characteristic absorption bands corresponding to P–O–P bonds could be observed at 1106, 996 and 520 cm^{-1}, indicating that the residual char contains phosphate or other phosphorus oxides [57]. The absorption peaks at 1639, 1300 and 759 cm^{-1} are assigned to P–O–Ph bonds in carbonized networks [10]. This implies the formation of heteroaromatic and polyaromatic compounds, where the phosphorus atoms play a role of crosslinking point to connect with different aromatic species and

Table 2
The TGA data and flammability characteristics of the DGEBA/*LPN*–EP thermosets.

Thermosetting system	Phosphorus content (wt %)	N_2 atmosphere			Air atmosphere			LOI value (vol %)	Flammability from vertical burning tests			
		T_{onset} (°C)	T_{max} (°C)	Char yield at 750 °C (wt %)	T_{onset} (°C)	T_{max} (°C)	Char yield at 750 °C (wt %)		UL–94 classification	Flaming drips	Total flaming time (sec)	Maximal flaming time (sec)
Pure DGEBA	0	343.45	384.54	3.70	304.59	375.09	0.63	22.31	Failed	Yes	>250	>50
DGEBA + 10 wt % LPN–EP	1.15	285.14	329.71	21.08	284.83	333.13	9.73	26.24	V-1	None	130.7	28.9
DGEBA + 20 wt % LPN–EP	2.31	273.51	317.71	24.34	271.83	311.93	14.37	28.45	V-1	None	72.8	17.1
DGEBA + 30 wt % LPN–EP	3.46	260.27	306.63	31.45	259.62	312.08	21.32	31.82	V-0	None	27.5	7.2
Error	–	±1.0	±1.0	±0.5	±1.0	±1.0	±0.5	±0.50	–	–	±2.5	±0.5

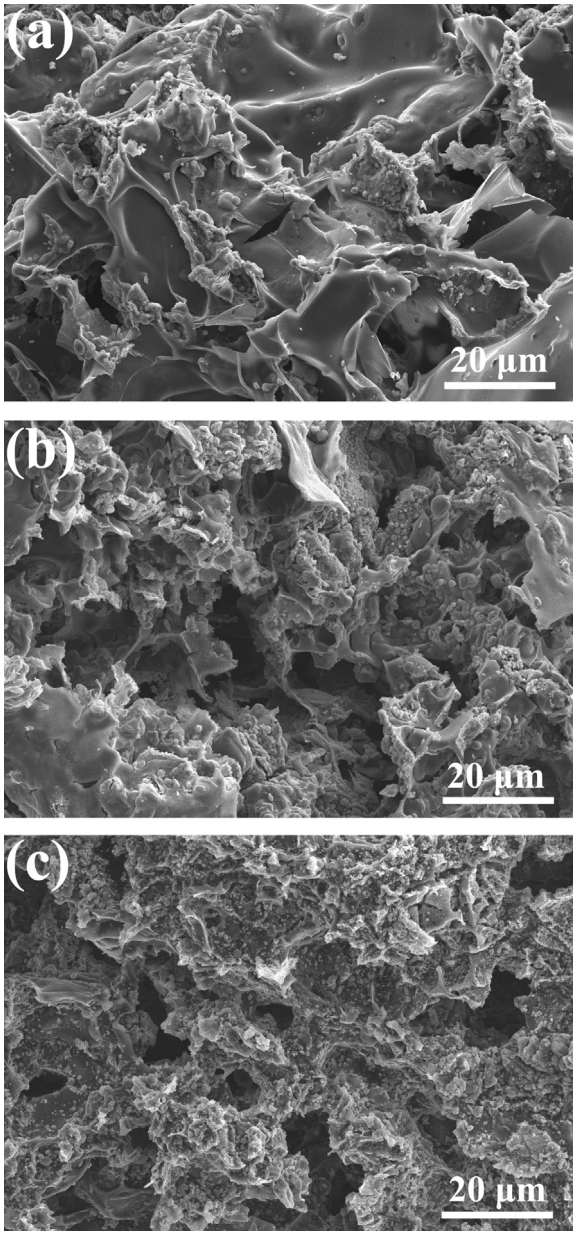

Fig. 13. SEM micrographs of the residual char collected from the burning-tested specimens of the DGEBA/*LPN*–EP thermosets containing (a) 10 wt %, (b) 20 wt %, and (c) 30 wt % of *LPN*–EP.

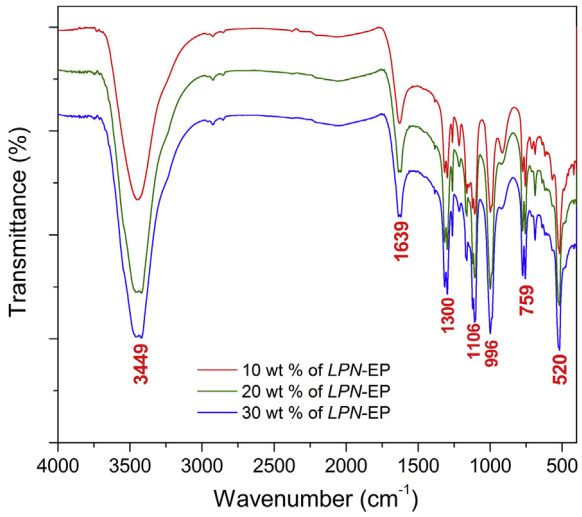

Fig. 14. FTIR spectra of the residual char for the DGEBA/*LPN*–EP thermosets.

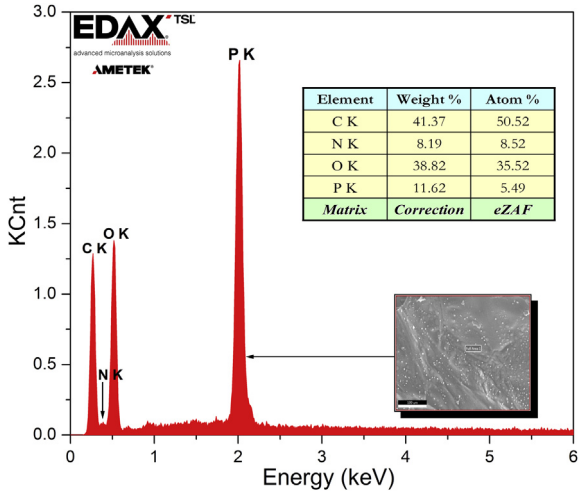

Fig. 15. EDX spectrum of the residual char of the DGEBA/*LPN*–EP thermoset containing 30 wt % of *LPN*–EP.

thus reinforce the char layer. The EDX spectrum determined an abundant elemental composition of carbon and phosphorus for the residual char as shown in Fig. 15. Furthermore, the solid-state ^{13}C NMR spectrum of the residual char presents a strong singlet resonance signal at 128 ppm, which is assigned to multi-aromatic C–C bonds as shown in Fig. 16. These results confirm the formation of phosphorus-rich carbonaceous char layers. In summary, the *LPN*–EP significantly improved the flame retardant properties of the epoxy thermosets in the ways of both condensed and gaseous phases. In the condensed phase, the thermo-oxidative reaction of polyphosphazene segments with the other ones can form the intumescent and phosphorus-rich carbonaceous char layers to prevent gaseous products from diffusing to the flame and to shield the polymer surface from heat and air during combustion. Meanwhile, the pyrolysis of the polyphosphazene segments produces

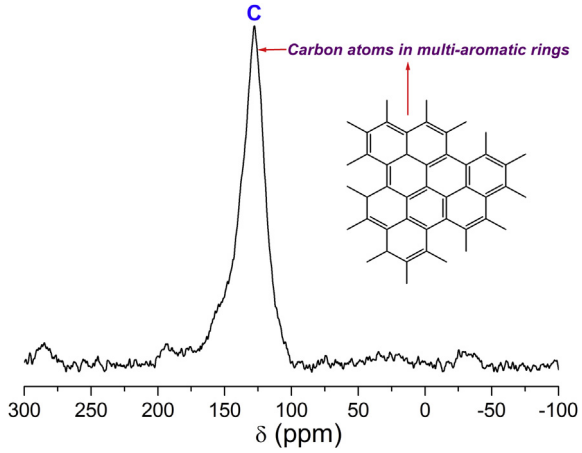

Fig. 16. Solid-state ^{13}C NMR spectrum of the residual char for the DGEBA/*LPN*–EP thermoset containing 30 wt % of *LPN*–EP.

phosphoric or polyphosphoric acid, which can promote the char formation. In the condensed phase, the polyphosphazene segments can release the nonflammable gases such as CO_2, NH_3, and N_2 during combustion to dilute the hot atmosphere, to cut off the supply of oxygen, and to cool the pyrolysis zone at the combustion surface. As a result, the DGEBA/*LPN*–EP thermosets achieved excellent flame-resistant performance.

4. Conclusions

The novel *LPN*–EP was successfully obtained through six-step reactions, and its chemical structures were confirmed by ^{1}H and ^{31}P NMR spectroscopy and FTIR. The halogen-free flame-retardant thermosetting systems consisting of DGEBA and *LPN*–EP were prepared, and their curing conditions were derived from the non-isothermal curing behaviors obtained by dynamic DSC scans. The resulting thermosets achieved good flame retardant properties with a self-extinguishing UL–94 V-0 flame rating. Such an extraordinary nonflammability is attributed to the synergistic effect from the unique phosphorus–nitrogen combination in *LPN*–EP segments. The thermosets also obtained a remarkable improvement in impact toughness due to the incorporation of rubber *LPN*–EP. With the features of high impact toughness and excellent flame resistance, the *LPN*–EP designed in this work shows a highlighted potential for electronic and microelectronic applications.

Acknowledgment

The financial support from the National Natural Science Foundation of China (Project Grant No.: 51173010 and 50973005) is gratefully acknowledged.

References

[1] Barontini F, Marsanich K, Petarca L, Cozzani V. Thermal degradation and decomposition products of electronic boards containing BFRs. Ind Eng Chem Res 2005;44(12):4186–99.
[2] Toldy A, Szolnoki B, Marosi G. Flame retardancy of fiber-reinforced epoxy resin composites for aerospace applications. Polym Degrad Stab 2011;96(3):371–6.
[3] Barontini F, Cozzani V, Petarca L. Calorimetric and kinetic analysis of the diglycidyl ether of the bisphenol A/tetrabromobisphenol A reaction for the production of linear brominated epoxy resins. Ind Eng Chem Res 2000;39(4):855–63.
[4] Gu JW, Zhang GC, Dong SL, Zhang QY, Kong J. Study on preparation and fire-retardant mechanism analysis of intumescent flame-retardant coatings. Surf Coat Technol 2007;201(18):7835–41.
[5] Barontini F, Cozzani V, Petarca L. Thermal stability and decomposition products of hexabromocyclododecane. Ind Eng Chem Res 2001;40(15):3270–80.
[6] Guo JY, Guo J, Xu ZM. Recycling of non-metallic fractions from waste printed circuit boards: a review. J Hazard Mater 2009;168(2–3):567–90.
[7] Uddin MA, Bhaskar T, Kusaba T, Hamano K, Muto A, Sakata Y. Debromination of flame retardant high impact polystyrene (HIPS–Br) by hydrothermal treatment and recovery of bromine free plastics. Green Chem 2003;5:260–3.
[8] Wang GA, Cheng WM, Tu YL, Wang CC, Chen CY. Characterizations of a new flame-retardant polymer. Polym Degrad Stab 2006;91(12):3344–53.
[9] Bras ML, Vilkie CA, Bourbigot S. Fire retardancy of polymers: new applications of mineral fillers. Cambridge: The Royal Society of Chemistry; 2005.
[10] Qian XD, Song L, Jiang SH, Tang G, Xing WY, Wang BB, et al. Novel flame retardants containing 9,10-dihydro-9-oxa-10-phosphaphenanthrene-10-oxide and unsaturated bonds: synthesis, characterization, and application in the flame retardancy of epoxy acrylates. Ind Eng Chem Res 2013;52(22):7307–15.
[11] Liao FH, Zhou L, Ju YQ, Yang YY, Wang XL. Synthesis of a novel phosphorus-nitrogen-silicon polymeric flame retardant and its application in poly(lactic acid). Ind Eng Chem Res 2014;53(24):10015–23.
[12] Liu R, Wang XD. Synthesis, characterization, thermal properties and flame retardancy of a novel nonflammable phosphazene-based epoxy resin. Polym Degrad Stab 2009;94(4):617–24.
[13] Chen HB, Zhang Y, Chen L, Shao ZB, Liu Y, Wang YZ. Novel inherently flame-retardant poly(trimethylene terephthalate) copolyester with the phosphorus-containing linking pendent group. Ind Eng Chem Res 2010;49(15):7052–9.
[14] Schartel B, Braun U, Balabanovich AI, Artner J, Ciesielski M, Döring M, et al. Pyrolysis and fire behaviour of epoxy systems containing a novel 9,10-dihydro-9-oxa-10-phosphaphenanthrene-10-oxide-(DOPO)-based diamino hardener. Eur Polym J 2008;44(3):704–15.
[15] Yoshioka-Tarver M, Condon BD, Cintrón MS, Chang S, Easson MW, Fortier CA, et al. Enhanced flame retardant property of fiber reactive halogen-free organophosphonate. Ind Eng Chem Res 2012;51(34):11031–7.
[16] Klinkowski C, Wagner S, Ciesielski M, Döring M. Bridged phosphorylated diamines: synthesis, thermal stability and flame retarding properties in epoxy resins. Polym Degrad Stab 2014;106:122–8.
[17] Tang QB, Wang BB, Shi YQ, Song L, Hu Y. Microencapsulated ammonium polyphosphate with glycidyl methacrylate shell: application to flame retardant epoxy resin. Ind Eng Chem Res 2013;52(16):5640–7.
[18] Schartel B, Balabanovich AI, Braun U, Knoll U, Artner J, Ciesielski M, et al. Pyrolysis of epoxy resins and fire behavior of epoxy resin composites flame-retarded with 9,10-dihydro-9-oxa-10-phosphaphenanthrene-10-oxide additives. J Appl Polym Sci 2007;104(4):2260–9.
[19] Shieh JY, Wang CS. Effect of the organosphosphate structure on the physical and flame-retardant properties of an epoxy resin. J Polym Sci Part A Polym Chem 2002;40(3):369–78.
[20] Toldy A, Tóth N, Anna P, Marosi G. Synthesis of phosphorus-based flame retardant systems and their use in an epoxy resin. Polym Degrad Stab 2006;91(3):585–92.
[21] Ho T-H, Hwang H-J, Shieh J-Y, Chung M-C. Thermal, physical and flame-retardant properties of phosphorus-containing epoxy cured with cyanate ester. React Funct Polym 2009;69(3):176–82.
[22] Qian XD, Song L, Hu Y, Yuen RKK, Chen LJ, Guo YQ, et al. Combustion and thermal degradation mechanism of a novel intumescent flame retardant for epoxy acrylate containing phosphorus and nitrogen. Ind Eng Chem Res 2011;50(4):1881–92.
[23] Perret B, Schartel B, Stöß K, Ciesielski M, Diederichs J, Döring M, et al. A new halogen-free flame retardant based on 9,10-dihydro-9-oxa-10-phosphaphenanthrene-10-oxide for epoxy resins and their carbon fiber composites for the automotive and aviation industries. Macromol Mater Eng 2011;296(1):14–30.
[24] Shree Meenakshi K, Pradeep Jaya Sudhan E, Ananda Kumar S, Umapathy MJ. Development and characterization of novel DOPO based phosphorus tetraglycidyl epoxy nanocomposites for aerospace applications. Prog Org Coat 2011;72(3):402–9.
[25] Wang XD, Zhang Q. Synthesis, characterization, and cure properties of phosphorus-containing epoxy resins for flame retardance. Eur Polym J 2004;40(2):385–95.
[26] Kahraman MV, Kayaman-Apohan N, Arsu N, Güngör A. Flame retardance of epoxy acrylate resin modified with phosphorus containing compounds. Prog Org Coat 2004;51(3):213–9.
[27] Allcock HR. Recent advances in phosphazene (phosphonitrilic) chemistry. Chem Rev 1972;72(4):315–56.
[28] Allcock HR. Recent developments in polyphosphazene materials science. Curr Opin Soild State Mater Sci 2006;10(5–6):231–40.
[29] Allcock HR. New approaches to hybrid polymers that contain phosphazene rings. J Inorg Organomet Polym Mater 2007;17(2):349–59.
[30] Jaeger RD, Gleria M. Poly(organophosphazene)s and related compounds: synthesis, properties and applications. Prog Polym Sci 1998;23(2):179–276.
[31] Liu H, Wang XD, Wu DZ. Novel cyclotriphosphazene-based epoxy compound and its application in halogen-free epoxy thermosetting systems: synthesis, curing behaviors, and flame retardancy. Polym Degrad Stab 2014;103:96–112.
[32] Sun J, Wang XD, Wu DZ. Novel spirocyclic phosphazene-based epoxy resin for halogen-free fire resistance: synthesis, cuing behaviors, and flammability characteristics. ACS Appl Mater Interfaces 2012;4(8):4047–61.
[33] Liu J, Tang JY, Wang XD, Wu DZ. Synthesis, characterization and curing properties of a novel cyclolinear phosphazene-based epoxy resin for halogen-free flame retardancy and high performance. RSC Adv 2012;2:5789–99.
[34] Xu GR, Xu MJ, Li B. Synthesis and characterization of a novel epoxy resin based on cyclotriphosphazene and its thermal degradation and flammability performance. Polym Degrad Stab 2014;109:240–8.
[35] Sun J, Yu ZY, Wang XD, Wu DZ. Synthesis and performance of cyclomatrix polyphosphazene derived from trispiro-cyclotriphosphazene as a halogen-free nonflammable material. ACS Sustain Chem Eng 2014;2(2):231–8.
[36] Bai YW, Wang XD, Wu DZ. Novel cyclolinear cyclotriphosphazene-linked epoxy resin for halogen-free fire resistance: synthesis, characterization, and flammability characteristics. Ind Eng Chem Res 2012;51(46):15064–74.
[37] Málek J. The kinetic analysis of non-isothermal data. Thermochim Acta 1992;200:257–69.
[38] Roşu D, Caşcaval CN, Mustăţă F, Ciobanu C. Cure kinetics of epoxy resins studied by non-isothermal DSC data. Thermochim Acta 2002;383(1–2):119–27.
[39] Kissinger HE. Reaction kinetics in differential thermal analysis. Anal Chem 1957;29(11):1702–6.
[40] Málek J. Kinetic analysis of crystallization process in amorphous materials. Thermochim Acta 2000;355(1–2):239–53.
[41] Málek J. A computer program for kinetic analysis of non-isothermal thermoanalytical data. Thermochim Acta 1989;138(2):337–46.
[42] Senum GI, Yang RT. Rational approximations of the integral of the Arrhenius function. J Therm Calorim 1977;11(3):445–7.

[43] Šesták J. Study of the kinetics of the mechanism of solid-state reactions at increasing temperatures. Thermochim Acta 1971;3(1):1–12.
[44] Hu JH, Shan JY, Wen DH, Liu XX, Zhao JQ, Tong Z. Flame retardant, mechanical properties and curing kinetics of DOPO-based epoxy resins. Polym Degrad Stab 2014;109:218–25.
[45] Calabrese L, Valenza A. Effect of CTBN rubber inclusions on the curing kinetic of DGEBA–DGEBF epoxy resin. Eur Polym J 2003;39(7):1355–63.
[46] Gouri ME, Bachiri AE, Hegazi SE, Rafik M, Harfi AE. Thermal degradation of a reactive flame retardant based on cyclotriphosphazne and its blend with DGEBA epoxy resin. Polym Degrad Stab 2009;94(11):2101–6.
[47] Zhu SW, Shi WF. Thermal degradation of a new flame retardant phosphate methacrylate polymer. Polym Degrad Stab 2003;80(2):217–22.
[48] Allcock HR, Taylor JP. Phosphorylation of phosphazenes and its effects on thermal properties and fire retardant behavior. Polym Eng Sci 2000;40(5):1177–89.
[49] Devapal D, Packirisamy S, Reghunadhan Nair CP, Ninan KN. Phosphazene-based polymers as atomic oxygen resistant materials. J Mater Sci 2006;41(17):5764–6.
[50] Qian LJ, Ye LJ, Xu GZ, Liu J, Guo JQ. The non-halogen flame retardant epoxy resin based on a novel compound with phosphaphenanthrene and cyclotriphosphazene double functional groups. Polym Degrad Stab 2011;96(6):1118–24.
[51] Ciesielski M, Schäfer A, Döring M. Novel efficient DOPO-based flame-retardants for PWB relevant epoxy resins with high glass transition temperatures. Polym Adv Technol 2008;19(6):507–15.
[52] Braun U, Balabanvich AI, Schartel B, Knoll U, Artner J, Ciesielski M, et al. Influence of the oxidation state of phosphorus on the decomposition and fire behavior of flame-retarded epoxy resin composites. Polymer 2006;47(26):8495–508.
[53] Schäfer A, Seibold S, Walter O, Döring M. Novel high T_g flame retardancy approach for epoxy resins. Polym Degrad Stab 2008;93(2):557–60.
[54] Reed CS, Taylor JP, Guigley KS, Coleman MM, Allcock HR. Polyurethane/poly[bis(carboxylatophenoxy)phosphazene] blends and their potential as flame-retardant materials. Polym Eng Sci 2000;40(2):465–72.
[55] Qian LJ, Ye LJ, Qiu Y, Qu SR. Thermal degradation behavior of the compound containing phosphaphenanthrene and phosphazene groups and its flame retardant mechanism on epoxy resin. Polymer 2011;52(24):5486–93.
[56] Bai ZM, Song L, Hu Y, Yuen RKK. Preparation, flame retardancy, and thermal degradation of unsaturated polyester resin modified with a novel phosphorus containing acrylate. Ind Eng Chem Res 2013;52(36):12855–64.
[57] Varma HK, Suresh Babu S. Synthesis of calcium phosphate bioceramics by citrate gel pyrolysis method. Ceram Int 2005;31(1):109–14.